Journal of Asian Earth Sciences 312 (2026) 107341

Contents lists available at ScienceDirect

Journal of Asian Earth Sciences

journal homepage: www.elsevier.com/locate/jseaes

Seismotectonic aspects of the 2025 Kunar earthquake, Afghanistan: Insights from field observations and InSAR-based remote sensing

Zakeria Shnizai [a,b,*], Zhenjiang Liu [c], Richard T Walker [a], Hamidullah Waizy [d,e], Ekbal Hussain [f]

[a] Department of Earth Sciences, University of Oxford, South Parks Road, Oxford OX1 3AN, the United Kingdom of Great Britain and Northern Ireland
[b] St John's College, University of Oxford, Oxford OX1 3JP, The United Kingdom of Great Britain and Northern Ireland
[c] College of Geological Engineering and Geomatics, Chang'an University, Xi'an 710054, China
[d] Department of Earth Sciences, Durham University, Durham DH1 3LE, The United Kingdom of Great Britain and Northern Ireland
[e] Department of Geological Engineering and Exploration of Mines, Kabul Polytechnic University, Karta-e-Mamorin, Kabul, Afghanistan
[f] British Geological Survey, Nicker Hill, Keyworth, The United Kingdom of Great Britain and Northern Ireland

ARTICLE INFO

Keywords:
Active tectonics
Earthquake source parameters
InSAR and ground deformation
Landslides
Seismic hazard
Kunar-eastern afghanistan

ABSTRACT

Active deformation in eastern Afghanistan occurs across a complex fault network associated with the India-Eurasia collision zone, yet the role of subsidiary structures remains poorly constrained. The 31 August 2025 Mw 6.0 Kunar earthquake provides an opportunity to investigate their role within the Kunar Fault System. This earthquake caused severe damage to unreinforced masonry and mudbrick structures, triggered over 104 landslides, and generated > 22 aftershocks with M ≥ 4.0. The earthquake resulted from thrust faulting on the north-northwestern segment of the Kunar fault system within the Hindu Kush ranges. This fault system forms a broad deformation zone characterized by predominantly left-lateral to oblique motion, with reverse slip accommodated on subsidiary thrust faults, particularly along the northern margin of Kunar valley. Field investigations document widespread surface deformation along active thrust zones, including open ground cracks and landslides. Surface cracks are concentrated in Mazar-Dara Valley of the Nurgal District, where most landslides and casualties occurred. Ascending and descending InSAR interferograms reveal contrasting deformation patterns between the mainshock and a Mw 5.6 aftershock on 4 September 2025. The aftershock exhibits a compact deformation field, approximately elliptical in shape (~5 km × 9 km), and with a NEE-trending long axis consistent with reverse faulting on a moderate-sized structure. The peak Line-of-Sight displacement of ~ 15 cm was located west of Ghaziabad village, which is west of the mainshock. In contrast, the mainshock produced a broader (~12 km × 9 km) and spatially heterogeneous deformation field dominated by uplift with minor subsidence, reaching a maximum LOS displacement of ~ 22 cm east of Ghaziabad. The complexity of the mainshock deformation may reflect rupture involving structurally segmented or multiple fault strands, while the detailed geometry of the seismogenic fault remains to be further resolved by future geodetic fault modelling efforts.

1. Introduction

Eastern Afghanistan lies within the active collision zone between the Indian and Eurasian tectonic plates, where crustal deformation including shorting occurs across a complex network of major and subsidiary faults (Fig. 1a). Several major active faults have been mapped and characterized based on their distinct geomorphic expression in the landscape (e.g., Shnizai, 2020; Shnizai and Walker, 2024). However, the distribution of shallow crustal deformation and the role of subsidiary structures within the Kunar Fault System remain poorly constrained. Recent seismic events provide valuable opportunities to investigate the role of subsidiary structures within the Kunar Fault System. One such event occurred on 31 August 2025, at 23:47 local time, when a magnitude 6.0 shallow earthquake struck eastern Afghanistan at a depth of 8 km, with its epicentre located in Nurgul District, Kunar Province (Fig. 1a-1b). The earthquake caused severe shaking across Kunar, Nangarhar, Laghman, and Nuristan Provinces, leading to the collapse of mudbrick, adobe structures and unreinforced masonry homes. Infrastructure damage was severe, health facilities overwhelmed, and numerous water sources destroyed, leaving many communities without

* Corresponding author at: Department of Earth Sciences, University of Oxford, South Parks Road, Oxford OX1 3AN, UK.
E-mail address: zakeriashnizai@gmail.com (Z. Shnizai).

https://doi.org/10.1016/j.jseaes.2026.107341
Received 15 May 2026; Received in revised form 29 August 2026; Accepted 17 September 2026
Available online 18 September 2026
1367-9120/© 2026 The Author(s). Published by Elsevier Ltd. This is an open access article under the CC BY license (http://creativecommons.org/licenses/by/4.0/).

access to clean drinking water, sanitation, or hygiene supplies. The event also triggered numerous landslides that blocked critical roads, complicating rescue efforts. Casualty numbers were raised as responders reached remote villages isolated by landslides, debris, and frequent aftershocks. More than 22 aftershocks above magnitude 4.0, including a magnitude 5.6 on 4 September and a magnitude 4.9 on 23 September, further weakened structures and hindered access to steep mountainous regions (e.g., United Nations Satellite Centre (UNOSAT) 2025 and USGS 2025a) (Fig. 1b).

The Kunar earthquake resulted in devastating consequences, with local authorities reporting 2,205 fatalities, >3,600 injuries, and ~ 6,700 homes either destroyed or severely damaged. More than 500,000 people were affected, including 263,000 children (Afghanistan Capacities Project (ACAPS) 2025; OCHA (United Nations for the Coordination of Humanitarian Affairs) 2025; Reliefweb, 2025). Rapid assessments across the impacted districts revealed widespread housing destruction, thousands of displaced families, and critical child protection issues, including cases of orphaned and unaccompanied children. Additionally, the loss of livestock in Nangarhar and Kunar Provinces has further strained household livelihoods, exacerbating the earthquake's humanitarian and

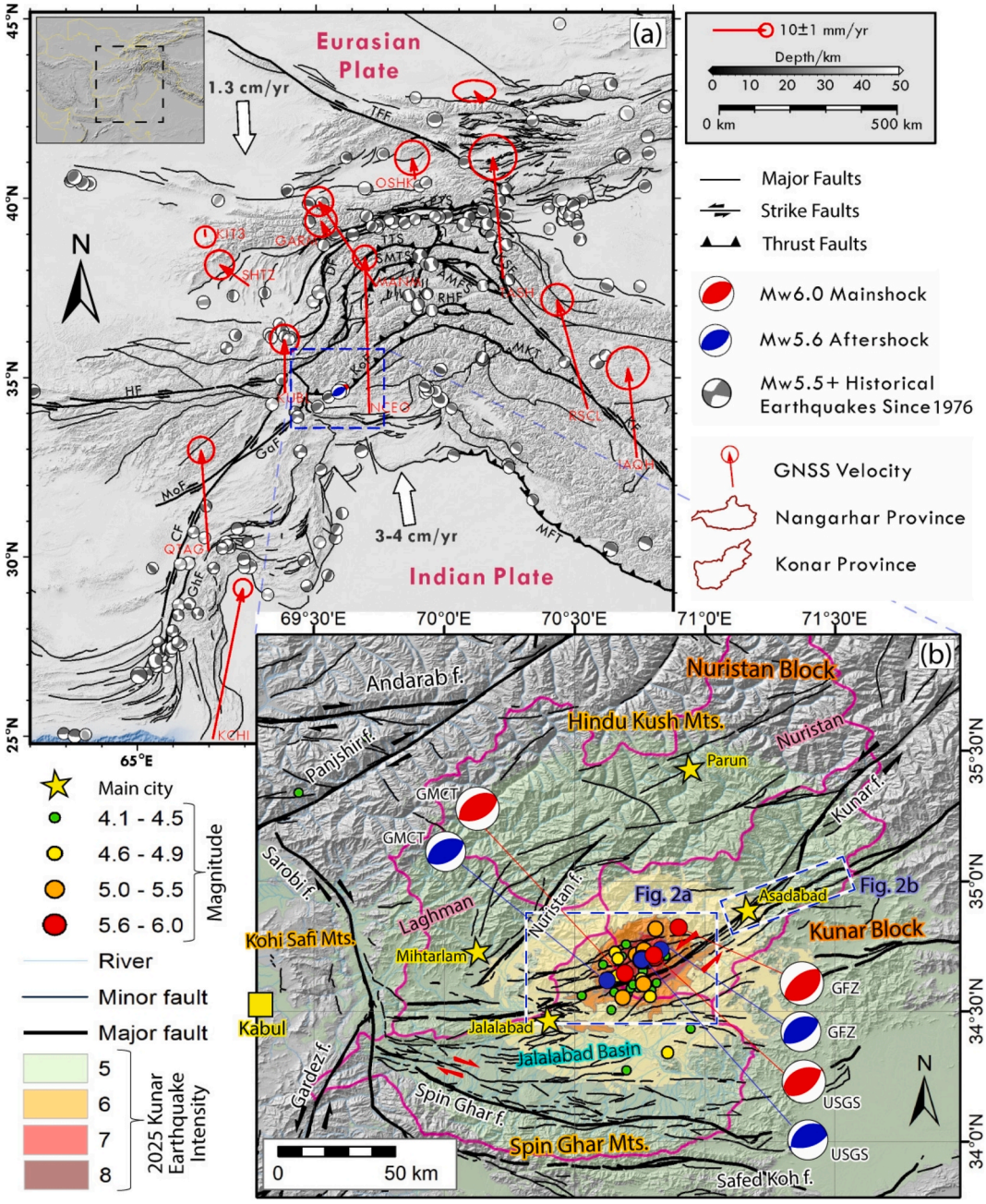


Fig. 1. (a) Tectonic setting of the study region, situated in the northern part of the India-Eurasian collision. Black solid lines represent major fault lines. The red vectors indicate GPS velocities relative to Eurasia (Mohadjer et al., 2010). Focal mechanisms, shown in grey, illustrate instrumentally recorded earthquakes with magnitudes greater than 5.5 since 1976 (Ekström et al., 2012). Abbreviation of faults: CF, Chaman fault; DF, Darvaz fault; GaF, Gardez fault; GhF, Ghazaband fault; HF, Herat fault; KSF, Kongur Shen fault; MoF, Mokur fault; KoF, Kunar fault; MFT, Main Frontal Thrust; KF, Karakoram fault; MKT, Main Karakoram Thrust; RHF, Reshun-Hunza fault; AMFS, Aksu-Murghab fault system; SMTS, Sarez-Murghab thrust system; TTS, Tanymas thrust system; TFF, Talas-Fergana fault; PTS, Pamir thrust system. The active faults are modified from Shnizai (2020). (b) Location of the August 31 mainshock (Mw 6.0) and its aftershocks in eastern Afghanistan. Pink dashed lines represent eastern provinces boundaries. The figure location is marked by a blue dashed rectangle in Fig. 1a. Background SRTM DEMs from Farr et al. (2007).

economic impacts (Fig. 1b).

The 2025 Kunar earthquake marks another devastating seismic event in Afghanistan, following the June 2022 earthquake Paktika-Khost in southeastern Afghanistan, and the 2023 Herat earthquake sequence in the western part of the country. Unlike the Herat earthquake sequence, the 2025 Kunar earthquake struck within the highly active Hindu Kush fold-and-thrust belt in eastern Afghanistan. The epicentral region is situated approximately 40 km northeast of Jalalabad and 38 km southwest of Asadabad (Fig. 1a-1b). This area lies within steep, high-relief terrain, where snow-capped peaks are continually modified by active tectonics and surface processes, including fluvial, aeolian, and glacial erosion. The landscape is characterized by deeply incised valleys and rugged ridges, shaped by protracted deformation associated with the India-Eurasia collision. Toward the Kunar River and the Jalalabad Basin, the terrain transitions into a piedmont zone composed of alluvial deposits.

Recent studies of the August 31st 2025 Kunar Earthquake have investigated its surface deformation using InSAR and teleseismic waveform modelling (He et al., 2026), and documented its damage patterns, geotechnical effects, and surface deformation using field and remote-sensing observations (Alluqmani et al., 2026; Ansari et al., 2025; Shirzaei et al., 2025; Torabi et al., 2026). Despite these important contributions, the relationship between the region fault architecture, geomorphic expression of active faults, coseismic deformation, and observed earthquake impacts remain poorly constrained. In particular, it remains still unclear how the observed coseismic deformation relates to the main Kunar Fault and the role of subsidiary structures, predominantly in the northern part of the Kunar Valley within the Nuristan Block, in accommodating shallow deformation. Specifically, a comprehensive seismotectonic assessment integrating field observations, satellite-derived geomorphic mapping, optical imagery, and InSAR data have not yet been undertaken.

To address this research gap, this study aims to investigate the coseismic surface deformation caused by the 31 August 2025 Kunar earthquake, interpret its tectonic context, assess structural damage patterns, and explore its broader geodynamic implications, as well as its role in the tectonics of eastern Afghanistan. The location and orientation of the Kunar fault system were mapped and analysed using the Shuttle Radar Topography Mission (SRTM) 1-arcsecond anaglyph images, Landsat 8 data, Bing Aerial, ESRI basemap, and freely available resources from Google Earth. Despite the severe impacts of the event, direct evidence of surface deformation remains scarce because the affected mountainous terrain is remote and field investigations have been limited. Under such conditions, satellite-based geodetic observations, particularly Interferometric Synthetic Aperture Radar (InSAR), provide a powerful means of quantifying surface deformation. Here, we integrate InSAR measurements with fault mapping from optical imagery and conducted field investigations to jointly characterize the spatial extent and magnitude of displacement and to link deformation patterns with active structures, damage distribution, and landslide occurrence.

2. Tectonic setting and seismicity

Afghanistan lies within the Alpine-Himalayan orogenic belt, formed by the collision of the Arabian, Indian, and Eurasian plates over the past 55 million years (Treloar and Izatt, 1993). This tectonic activity has caused crustal thickening and uplift in eastern and northeastern Afghanistan, forming regional highlands and inverting prior tectonic relief such as in the Hindu Kush and Pamir Ranges (Shnizai et al., 2024, 2022; Tapponnier et al., 1981). Ongoing deformation, including strike-slip faulting and shortening along thrust faults, continues in structures like the Sulaiman Folded Region, Spin Ghar Mountains, Hindu Kush and Salt Ranges (Denikaev et al., 1972; Nakata et al., 1991; Shnizai et al., 2022; Verma et al., 1980). Eastern and northeastern Afghanistan is one of the most seismically active regions in the country, frequently experiencing moderate to large earthquakes (e.g., Abdrakhmatov et al., 2024; Akhundzadah, 2024; Ambraseys and Bilham, 2003; Dewey, 2006; Mohammadi et al., 2026; Shnizai, 2020; Shnizai and Walker, 2024), such that the eastern and northeastern parts of the country have significant seismic hazard (e.g., Quittmeyer & Jacob 1979; Shnizai & Walker 2024) (Fig. 1a).

Eastern Afghanistan encompasses the provinces of Kunar, Nangarhar, Laghman, and Nuristan, characterized by transpression tectonics and featuring a range of faults with varying orientations (Fig. 1b). The region is cut by major active faults, including the Chaman, Paghman, Gardez, Panjshir, Spin Ghar and Kunar faults (e.g., Abdullah et al., 2008; Shnizai, 2020; Waizy et al., 2025) (Fig. 1a, 2a). The Chaman Fault, with a slip rate of 5–35 mm/yr, exhibits the most prominent evidence of seismic activity. It is characterized by a combination of creeping and locked segments with varying levels of seismic activity across the different segments (Beun et al., 1979; Furuya and Satyabala, 2008; Shnizai et al., 2024, Shnizai et al., 2020). Eastern Afghanistan is home to two significant mapped active fault systems: the Spin Ghar Fault System and the Kunar Fault System. The Spin Ghar fault system is one of the major groups of active structures in eastern Afghanistan, stretching ~ 130 km east–west direction along the Spin Ghar Mountains in the Jalalabad Basin (Shnizai and Walker, 2024). The fault system includes a group of strike-slip and oblique-slip thrust fault strands only 25 km from Jalalabad City (Fig. 1a, 2a). The Kunar fault, which separates the Nuristan tectonic block from the Kunar Zone to the north-northeast, stretches from Kabul's Sarobi district along the Kabul and Kunar River Valleys to the Chitral Region (Shnizai, 2020). The geomorphic expression of the Kunar fault system is similar to those faults that are present in the Jalalabad Basin. According to Prevot et al. (1980), the Kunar Fault appears to represent a significant suture zone, potentially marking the boundary between an island arc and the Asian continent.

There are no clear documents or historical records of earthquakes on the Kunar fault, but microseismicity records show that the Kunar and Spin Ghar faults are active with a predominant left-lateral sense of motion (Prevot et al., 1980). On February 19, 1842, an earthquake with a magnitude of 7.5 struck Eastern Afghanistan at an unknown depth, causing hundreds of fatalities (Dewey, 2006; Heuckroth and Karim, 1970). According to Dewey (2006), the earthquake's epicentre was located in the Peach District of Kunar, while Ambraseys and Bilham (2014) reported it as being on the right bank of the Kabul River in Jalalabad City. The earthquake, along with its aftershocks, inflicted severe damage in Jalalabad and one-third of the houses were destroyed, blocking streets and leaving residents without escape routes. Beyond the city walls, near the river, the ground cracked open, releasing water onto the surface. According to Baird-Smith (1942), the seismic activity caused the water of the Kabul River to be twice thrown from its bed, disrupting the surrounding areas and highlighting the immense power of the earthquake. In the Kunar Valley, landslides triggered by the earthquake led to the destruction of two forts. The microseismicity and historical earthquakes indicate that faults in eastern Afghanistan are active. Their distribution offers insight into potential future earthquake locations, highlighting areas where modern stresses are sufficient to trigger fault slip.

3. Materials and methods

3.1. Remote-sensing data and field investigations

This study integrates multi-source datasets to map active faults, quantify coseismic surface deformation, and assess secondary geological effects associated with the 2025 August 31st Kunar earthquake and its subsequent aftershocks in eastern Afghanistan. Regional mapping of active faults in the northern Kunar Valley, the site of the Mw 6.0 mainshock and subsequent aftershocks was undertaken using 30-m Landsat 8 Operational Land Imager (OLI) multispectral satellite images and 1-arcsecond SRTM digital elevation data (DEM) (obtained from obtained from the U.S. Geological Survey portal https://earthexplorer.

usgs.gov), supplemented by high-resolution optical satellite imagery as available through ESRI basemap, Bing Aerial, and Google Earth. The SRTM 30-m DEM were processed using SimpleDEMViewer (https://www.jizoh.jp/) to generate anaglyph images of the study area (Shnizai, 2020). We used red-cyan glasses to visualize and interpret tectonic geomorphic features. In addition, shaded-relief, slope and topographic maps were employed to delineate active fault traces and evaluate their geomorphic expression across the landscape.

Fieldwork complemented the remote sensing analyses through direct measurements and mapping of surface cracks, fault-related deformation, and earthquake-induced landslides. Fieldwork investigations place between 9 and 15 September 2025 within the accessible epicentral area (green dashed outline in Fig. 2a) to document earthquake-induced ground deformation, active fault geomorphology, and ground cracks along the mapped Kunar Fault System. Access to the remaining study area was restricted due to rugged terrain and roads that had been

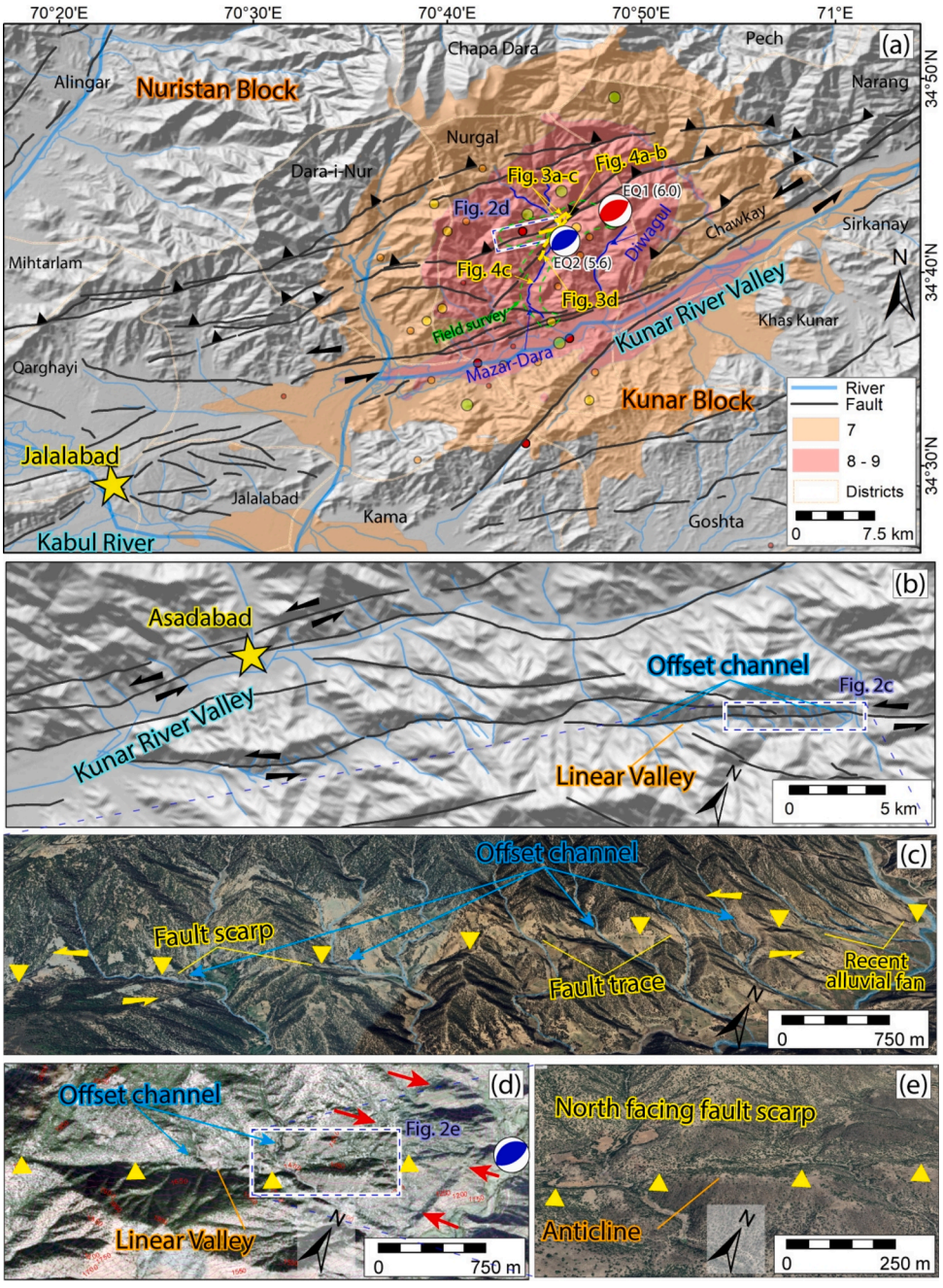


Fig. 2. (a) SRTM 1-arcsecond hillshade map (e.g., Farr et al., 2007) showing the epicentral area of the August 31st earthquake and the Kunar fault system. Red beachball symbols represent the focal mechanism of the 2025 mainshock (Mw 6.0), while blue beachball symbols indicate the aftershock (Mw 5.6), as reported by the USGS. Red colour represents intensity 7 and 8 as shown in Fig. 1b. Yellow lines indicate the location of surface cracks on bedrock terrain. (b) Enlarged localized images of the northeastern section of the Kunar fault system, highlighting multiple fault strands. Location shown in the upper panel of figure 1b. (c) Google Earth 3D view illustrating consistent streams that exhibit left-lateral offsets along the main Kunar fault near Asadabad City. Image from Google Earth Pro, imagery © 2026 Airbus, accessed January 2026. (d) Thrust fault trace overlaid on the ESRI Basemap with contour lines, showing the location of a seismic events accompanied by left-lateral stream offsets. The fault trace is distinctly visible, dipping northward. Image is from: Esri, DigitalGlobe, GeoEye, i-cubed, USDA FSA, USGS, AEX, Getmapping, Aerogrid, IGN, IGP, swisstopo, and the GIS User Community. (e) A broader view of the thrust fault displayed in Fig. 2d. Yellow triangles mark the positions of the fault traces.

damaged. A second survey (25–27 October 2025) focused on earthquake-related building damage and landslide impacts; however, many of the previously observed ground cracks had been obscured due to monsoon rainfall and subsequent erosion. We identified ground cracks by analysing their fresh morphology, linear continuity, and spatial relationship with the mapped fault traces. In addition, a post-event landslide inventory from the Copernicus Emergency Management Service (CEMS) Rapid Mapping products (EMSR839) was incorporated to support the assessment of earthquake-induced landslide hazards and damage patterns. The inventory was generated shortly after the event through the interpretation of high-resolution pre- and post-event optical satellite imagery to complement field observations. Accessible landslide sites were also visited to document representative failures and verify the mapped inventory.

3.2. Sentinel-1 InSAR data and processing

Sentinel-1 Interferometric Synthetic Aperture Radar (InSAR) data were processed to generate coseismic interferograms, enabling the quantification of line-of-sight (LOS) surface deformation across the epicentral region. Benefiting from a revisit frequency of 6 to 12 days by the Sentinel-1 satellite mission over tectonically active regions worldwide (Elliott et al., 2016; Li et al., 2016; Liu et al., 2025), we are able to separate the co-seismic deformation associated with the Mw 6.0 mainshock EQ1 and the subsequent Mw 5.6 aftershocks EQ2 (Table 1). We collected Sentinel-1 Synthetic Aperture Radar (SAR) images (Table 2) from ascending track T173 and descending track T005, provided by the European Space Agency and applied interferometric SAR (InSAR) techniques to derive the co-seismic surface deformation from the Mw 6.0 (August 31) mainshock and Mw 5.6 (September 4) aftershock (see Section 4.2).

The SAR data from all four tracks were processed using the GAMMA software (Wegnüller et al., 2016) to retrieve the co-seismic displacements. In the processing flow, the Precise Orbit Ephemerides from ESA were used to correct for orbital effects. The SRTM 1-arcsecond (~30 m) digital elevation model was employed for co-registration and topographic phase removal in the interferograms (Farr et al., 2007). To avoid potential phase jumps in the azimuth of the SAR data, a rigorous co-registration strategy is required to achieve co-registration accuracy exceeding 0.001 pixels (Yague-Martinez et al., 2016). In the co-registration process, a DEM-assisted alignment method is first applied to perform coarse alignment, followed by iterative refinement using sub-pixel offsets. Finally, a spectral diversity algorithm (Scheiber and Moreira, 2000) is used to achieve refined alignment of the overlapping area of two bursts. Interferograms are then multi-looked by a factor of 10 in range and 2 in azimuth, effectively resulting in approximately 50 m square pixels. The interferograms are filtered by the adaptive phase filter (Goldstein et al., 1988) to reduce phase noise. Before phase unwrapping, pixels with interferometric coherence lower than 0.4 were masked out to reduce unreliable phase signals and improve the robustness of phase unwrapping. The SNAPHU unwrapping method (Chen and Zebker, 2001) was utilized to retrieve the LOS surface displacements. To mitigate atmospheric errors (especially tropospheric delays) on the interferograms, the Generic Atmospheric Correction Online Service for InSAR (GACOS) (Yu et al., 2018b, Yu et al., 2018a, Yu et al., 2017) is used for atmospheric error estimation and correction. Finally, we retrieved the InSAR line-of-sight (LOS) surface deformation fields for the Mw 6.0 mainshock and the Mw 5.6 aftershock (see Section 4.2).

4. Results

4.1. Kunar fault system and its subsidiary faults

The Kunar Fault runs parallel to the Kunar Valley, extending over 200 km in length, with an oblique left-lateral displacement (Fig. 1a, 2a-2b). The fault features northeast-trending, continuous to discontinuous, and curved scarps located at the southern front of the Hindu Kush Ranges, cutting across bedrock, alluvial fans, landslide deposits, and other recent geological formations (Fig. 2a). We observed shutter ridges, displaced and beheaded stream channels, as well as offset alluvial fans and springs. Along much of its length, the fault runs through the Kunar Valley, characterized by a low relief plain situated between the Kunar tectonic block and Nuristan fault block, which shaped the course of the main Kunar River and its tributaries (Fig. 2a). In the southwestern part of the fault in Jalalabad Basin, several alluvial and fluvial deposits are elevated by tens of meters to $\geq$ 200 m above the current river channel. These late Quaternary alluvial deposits, consisting of clay, sand, silt, and loess, are intersected by faults. These fans have been uplifted, causing the Kunar River to narrow significantly as it flows around the terraces from the northeast to the south and southwest, into the Kunar Valley before merging with the Kabul River in the Jalalabad Basin (Fig. 1b, 2a). The lower elevation of the alluvial deposits above the current riverbed suggests they are younger than the terraces at higher elevations. These

Table 1
Focal mechanism solutions for the Mw 6.3 and Mw 5.6 earthquakes in Eastern Afghanistan in August and September.

Event Date/(UTC)	Source	Location Lon (°)	Lat (°)	Focal Mechanism Depth (km)	Strike (°)	Dip (°)	Rake (°)		Mag (Mw)
EQ1 (Date: 2025/08/31, Time- 19:17:34)	GCMT	70.71	34.66	12	235 63	41 49	84 95		6.0
	GFZ	70.86	34.72	12	52 232	58 31	89 90		6.0
	USGS	70.793	34.706	8	251 48	41 52	108 75		6.0
EQ2 (Date: 2025/09/04, Time- 16:56:25)	GCMT	70.64	34.61	12	240 60	41 49	90 90		5.6
	GFZ	70.83	34.71	11	56 238	56 33	88 91		5.6
	USGS	70.791	34.719	10	228 74	32 61	67 103		5.6

Table 2
SAR imagery details using for co-seismic surface deformation analysis.

Event	Track	Primary scene (YYYYMMDD)	Secondary scene (YYYYMMDD)	Perp.B (m)	Heading Angle (°)	Incidence Angle (°)
EQ1	Asc173	20,250,820	20,250,901	−125.8	−13.075	39.543
	Des005	20,250,821	20,250,902	−61.3	193.044	39.561
EQ2	Asc173	20,250,901	20,250,907	82.1	−13.077	39.543
	Des005	20,250,902	20,250,908	−18.6	193.046	39.562

younger deposits are also covered by a thin layer of fluvial gravel and sand, originating from the surrounding mountains.

Along the northern part of the Kunar Valley, continuous ridges indicate an oblique sense of motion (Fig. 2a). Evidence of left-lateral offsets across the fault are less distinct to the south near Jalalabad Basin, possibly due to steep topography, active drainage systems, and increased human activities. However, along the fault and further northeast, the Kunar Fault zone exhibits very clear left-lateral offsets near the Asadabad City (Fig. 2a, 2c-2d). In this area, the fault has continuous, linear scarps cross bedrock terrain and recent alluvial fans trending parallel to the major Kunar Valley. The systematically deflected stream channels at varying distances serve as evidence of repeated and recent seismic activities along the Kunar fault in the area. The minimum offset observed is ~ 25 m in recent fans, while the maximum exceeds hundreds of meters.

The Kunar fault system is complex and constitutes several major and minor faults, forming a broad deformation zone between the Nuristan Fault Block and the Kunar Block (Fig. 1b, 2b). The dominant sense of motion along the fault is left-lateral to oblique, accompanied by reverse motion on smaller splay faults, particularly on the northern side within the Nuristan Block, which predominantly consists of bedrock and mountainous terrain (Fig. 2a). This has created a distributed system rather than a single fault line, with a complex geometry, with bends and splays that has caused strain partitioning and varying slip behaviour along both sides of the Kunar River Valley.

The 31 August 2025 Kunar earthquake resulted from thrust faulting on the north-northeastern segment of the main Kunar Fault system, within the Nuristan uplifted block of the southern Hindu Kush Range (Fig. 1a). Although the depth, location, and focal mechanism solutions for the earthquake sequence reported by GCMT (Global Centroid Moment Tensor), GFZ (German Research Centre for Geosciences), and USGS (U.S. Geological Survey) show some discrepancies, all events are consistently located within the uplifted area (Fig. 1b; Table 1). The rupture was followed by more than 22 aftershocks (Fig. 1b). The earthquake occurred close to or along thrust faults that we mapped from satellite imagery (Fig. 2a, 2d). The bedrock ridge within the epicentral area exhibits clear geomorphic evidence of contemporary deformation, and we believe the referenced faults within the uplifted area are responsible for the August 2025 earthquake (Fig. 2a, 2d-2e). This interpretation is supported by the InSAR deformation pattern (see Section 4.2). In the hanging wall, the fault splays into a pair of anticlines, which are distinctly expressed in the deformed land surface (Fig. 2d-2e). These tectonic geomorphic features indicate progressive growth of the uplifted area, initiating during the deposition of the gravel units and continuing through their subsequent incision by the river.

The active thrust faults in the epicentral area are predominantly north-verging and locally merge into a northeast-trending strike-slip fault zone (Fig. 2a). The minor thrust faults to the north are characterized by arcuate, discontinuous scarps on bedrock, primarily from the Paleogene to Carboniferous and Silurian periods. The structural control of the Kunar Valley is evident in the southward-flowing fluvial systems, which traverse both the thrust faults and the main Kunar Fault (Fig. 2a). This interaction has produced a series of fault types and orientations, with northeastward-oriented thrust faults that range from discontinuous to continuous arcuate range-bound and intermontane scarps.

Field surveys conducted after the two major events (Mw 6.0 and Mw 5.6) revealed widespread surface deformation along the thrust fault zones, particularly in the form of open cracks and landslides (Fig. 3a-3d, 4a-4d). These cracks predominantly followed east–west or northeast-southwest trends, with some reaching widths of up to 40 cm and showing very small vertical changes (Fig. 3b-3c). While most cracks were either continuous or discontinuous and visibly prominent across the landscape; however, the earthquake did not cause any significant crack displacements. Additionally, cracks observed in the deep valleys and steep slope areas may have been influenced by gravity-induced settling.

The cracks were concentrated along the Mazar-Dara Valley and, to a lesser extent, in the Diwagul Valley within the Nurgal District, the location of the earthquake's epicentre (Fig. 2a, 3a-3c). These two valleys also accounted for a large proportion of casualties, landslides and rock avalanches (Fig. 4a-4d). Prior to the mainshock, the region experienced heavy precipitation, leading to water-saturated slopes and erosion. The saturated soils were therefore, arguably, more prone to failure in the subsequent earthquake. The landslides triggered by the main earthquake and aftershocks primarily consisted of rockfalls and long-distance landslides along slopes with some cohesive soils. The rugged terrain characterized by steep slopes, high mountains, deep valleys, and dense forests, made field investigations challenging, limiting the ability to fully map the extent of surface deformation. Despite these difficulties, ground cracking, landslides, and rock avalanches were observed in multiple areas, underscoring the extensive impact of the seismic activity on the region's landscape.

4.2. *InSAR-derived coseismic deformation*

From the ascending and descending interferograms of both the mainshock and aftershock (Fig. 5a-5d), the 4 September Mw 5.6 aftershock exhibits a westward shift in deformation relative to the 31 August Mw 6.0 mainshock. This spatial migration suggests that the two events may represent cascading rupture along the same fault system, similar to the 2023 Herat earthquake sequence (Liu et al., 2025). The InSAR observations reveal contrasting deformation patterns for the two events.

The aftershock exhibits a relatively simple and compact deformation field characterized by an approximately elliptical shape, consistent with deformation expected for a moderate-magnitude reverse-faulting event (Fig. 5c-5d). The short axis of the ellipse is ~ 5 km, while the long axis extends ~ 9 km along a NEE direction, implying a fault striking NEE or SWW, which agrees with focal mechanism solutions reported by different agencies (Table 1). The deformation is dominated by LOS uplift, with a maximum LOS displacement of ~ 15 cm located west of Ghaziabad village and south of Oshunkan Alek village (Fig. 5c-5d). In contrast, the mainshock produces a more spatially heterogeneous deformation pattern that deviates from a simple elliptical geometry event (Fig. 5a-5b). The deformation is primarily characterized by LOS uplift accompanied by minor subsidence, with a maximum LOS displacement of ~ 22 cm. The affected area, approximately 12 km × 9 km, is concentrated around and east of Ghaziabad village (Fig. 5a-5b). The complexity of the deformation pattern may reflect rupture involving structurally segmented or multiple fault strands. However, the detailed geometry of the seismogenic fault cannot be fully resolved from the current InSAR observations alone and requires further quantitative geodetic fault modelling.

Given that focal mechanism solutions indicate NEE-SWW-striking faults for both events, we further constructed deformation profiles



Fig. 3. (a-d) Surface cracks observed following the August 31st mainshock and subsequent aftershocks north of the Kunar River Valley. The yellow triangle indicates the location of the surface cracks, most of which were identified in bedrock terrain. The locations of these photographs are shown in figure 2a.

across the inferred fault strike to better characterize the displacement gradients and infer possible dip directions (Fig. 5e-5f). The profiles from both ascending and descending tracks are not fully continuous, particularly in the near field where coherence is low. This decorrelation may reflect surface disruption associated with the earthquake, pre-event rainfall and flooding, or a combination of these factors. Reduced coherence may also introduce phase-unwrapping errors. In such conditions, longer-wavelength L-band SAR data may provide improved performance and could be incorporated in future studies. Despite these limitations, the InSAR data, together with the reverse-faulting focal mechanism solutions, provide useful first-order constraints on the rupture geometry. For the mainshock, both ascending and descending profiles show two uplift peaks in the near field, which may indicate deformation associated with two structurally segmented fault strands. The profile geometry is compatible with a north-dipping southern segment and a south-dipping northern segment. However, because no quantitative geodetic fault model is provided in this study and the near-field profiles are partly affected by decorrelation, this interpretation should be regarded as a first-order inference. Additional geodetic modelling will be required to further constrain the detailed fault geometry and slip distribution. In contrast, the aftershock profiles display a more symmetric single-peak displacement pattern, suggesting a relatively simpler deformation source. Additional geodetic modelling will be required to further constrain the fault geometry.

4.3. *Damage assessment and contributing factors*

The impacts of the Mw 6.0 earthquake and its aftershocks were also significantly exacerbated by human and systemic factors in eastern Afghanistan, resulting in a profound toll on both lives and communities. Following the earthquake sequence, the CEMS and United Nations Satellite Centre (UNOSAT) provided situational reporting and emergency mapping (EMSR839) (Copernicus 2025; Global Disaster Awareness and Coordination System (GDACS) 2025; UNOSAT 2025), covering 15 areas of interest (AOIs) both in Kunar and Nangarhar Provinces (Fig. 6a). The mapping revealed significant changes in land use and affected areas, using 30-cm Pleiades-Neo satellite imagery to compare pre- and post-event conditions in Kuz Kunar. In the worst-affected districts of Kunar, most mud-brick and stone houses collapsed, while damaged roads, power lines, and communication networks isolated many areas and made air transport the only reliable access option (Fig. 6b-5e). Nurgal District was the most severely affected, with ~ 427 houses destroyed, and 544 damaged (Fig. 6a). Chawkay District ranked second, with 41 buildings destroyed, 80 damaged, and 448 potentially damaged, followed by the Kuz Kunar and Dar-I Nur Districts. Significant impacts were also reported in Asadabad and Jalalabad cities, located nearly 40 km from the epicentral area (Fig. 6a).

One of the key factors contributing to the high number of casualties was the use of unreinforced adobe construction with traditional building methods, which left many buildings unable to withstand the earthquake (Fig. 6b-6c). In the epicentral region numerous houses are precariously built on steep slopes that cut into the mountains. These houses are constructed using rock and mud blocks mortared together with mud, which is mostly sandy and predominant in these mountainous areas (e.g., Fig. 6c, 7a). Although most houses feature flat roofs made of over 20 cm of dried mud supported by wooden beams, the mud-block or stone walls lack reinforcement to resist horizontal shaking (Fig. 6d-6e).

The construction of multi-story buildings often begins with a single



Fig. 4. **(a)** Landslide occurring in the Mazar Dara area. **(b)** Rockfall with large boulders triggered by an earthquake**. (c)** The depletion area or failure zone is visible after the landslide. **(d)** Landslides and rock avalanches were documented during an aftershock in Mazar Dara, Nurgal District.

story. As family populations grow, additional stories are added, first a second story, then a third (Fig. 7b). This approach poses significant technical challenges because the original design and wall thickness were intended to support only a single story. When the structure is expanded vertically, the insufficient wall thickness becomes a critical issue, affecting the building's stability and safety as it cannot bear a heavy load especially during seismic shaking. Additionally, half of the houses are built as dry stone masonry, with additional Pakhsa (rammed-earth construction) layers placed on top to complete the walls (Fig. 6d, 7b).

Afghanistan is a mountainous country where earthquakes often trigger secondary hazards such as landslides, which significantly increase damage and contribute to loss of life. For instance, in the Nurgal District's Mazar Dara Valley, over 104 landslides occurred, with most casualties resulting from these landslides (Fig. 7a). In nearly every village, most houses are constructed on steep terrains, often as multi-story buildings stacked closely together (Fig. 7c). Some villages have a history spanning nearly > 400 years and feature over 2,000 houses densely packed into a compact area of approximately 2,000 m2, with structures built closely together, often one atop another (e.g., Fig. 6b, 7c). During the earthquake, when a building collapsed at the base or was struck by a landslide or large rocks from above, neighbouring structures were unable to withstand the impact, leading to a chain reaction of collapses. Even during rescue operations, these pose significant challenges for teams to extract people from the ruins and debris.

Field observations reveal the emergence of new springs and increased discharge from existing water sources following the earthquake and its aftershocks. These hydrological changes are commonly associated with temporary increases in permeability caused by fracture openings and stress redistribution within the shallow crust. This suggests that the earthquake not only affected slope stability but also modified near-surface groundwater pathways. In the epicentral region steep slopes, rugged terrain, and high mountains have created highly

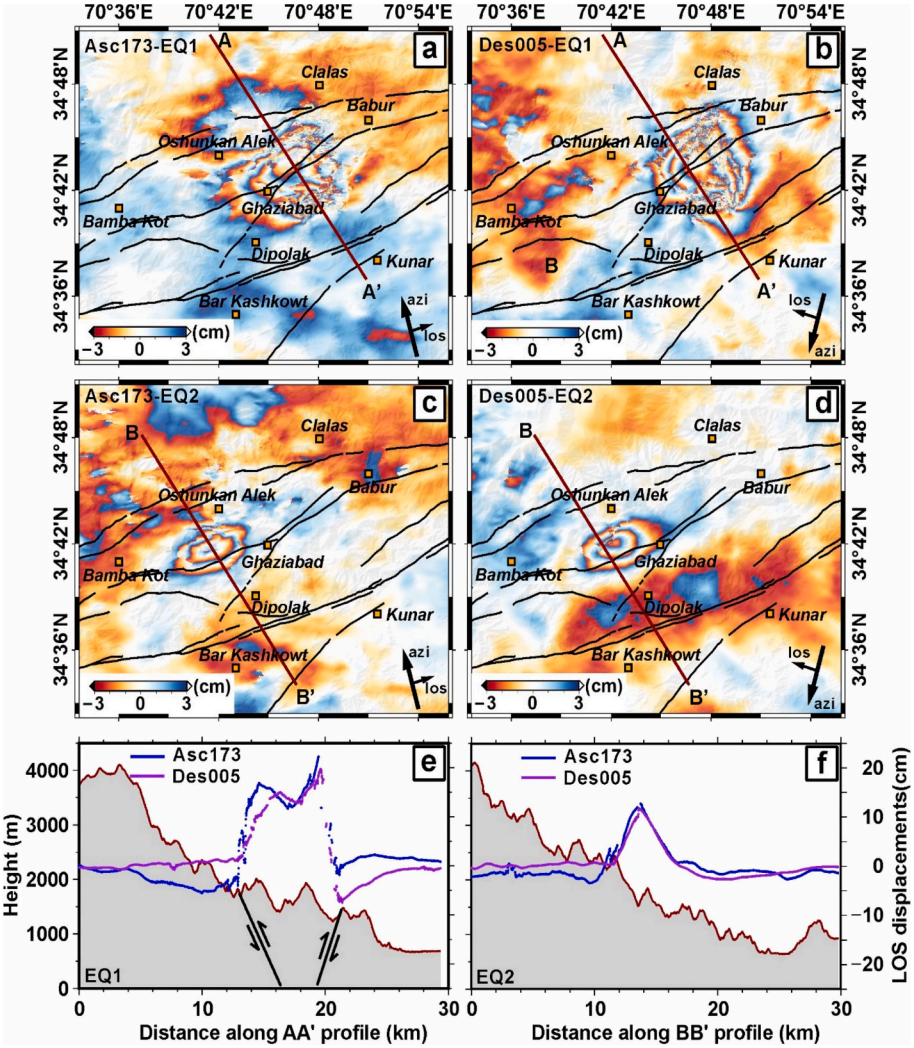


Fig. 5. Panels **(a-d)** show the ascending and descending Sentinel-1 InSAR coseismic interferogram with LOS deformation rewrapped to 6 cm fringes, with each cycle from red through white to blue indicating motion away from the satellite. Panels (**a-b**) correspond to the Mw 6.0 mainshock, while panels (**c-d**) show the Mw 5.6 aftershock that occurred on 4 September 2025. Panels **(e-f)** present the across-fault LOS deformation profiles extracted from the ascending and descending tracks for the two events. The blue and purple curves represent the ascending and descending observations, respectively. The shaded profile shows the topography.

unstable conditions where seismic shaking easily dislodges soil and rock, leading to rockfalls, debris flows, and large-scale slope failures. These risks were further intensified by heavy rainfall in the preceding days, which had weakened the ground, saturated soils, reduced slope stability, and transformed earthquakes into multi-hazard events involving new landslides and flash floods.

5. Discussion

5.1. Coseismal deformation and rupture characteristics

The 2025 August 31st earthquake and its aftershocks in eastern Afghanistan lie within the highest seismic hazard domain of the country, which has experienced repeated moderate to large damaging earthquakes driven by ongoing plate convergence (Fig. 8a). The mainshock and its largest aftershock on the 4 September resulted from thrust faulting in the Nuristan Block north of the main Kunar fault. Independent InSAR analyses of the 31 August 2025 earthquake indicate shallow thrust faulting with up to ~ 23 cm of LOS uplift near the epicentre, consistent with our results (~22 cm), whereas the Mw 5.6 aftershock produced a smaller maximum LOS uplift of ~ 17 cm (Shirzaei et al., 2025). He et al. (2026), using Sentinel-1 InSAR data and teleseismic waveform modelling, identified a complex, multi-stage rupture sequence involving the Mw 6.0 mainshock and three subsequent aftershocks exceeding Mw 5.0. Their findings revealed shallow faulting, widespread deformation, and surface displacements ranging from approximately 10 to 35 cm.

The uplift observed in the epicentral region aligns with the PS-InSAR findings of Torabi et al. (2026), who noted localized vertical uplift along mountain-front structures in Nuristan Block and subsidence in the adjacent Kunar Valley and Jalalabad Basin. These observations suggest that the 2025 Kunar earthquake sequence was characterized by structurally intricate deformation rather than a simple rupture along a single fault segment (He et al., 2026; Torabi et al., 2026).

5.2. Active fault architecture and deformation patterns

In Afghanistan, most recent destructive earthquakes that caused tens of thousands of casualties, including the 2002 Nahrin, 2022 Khost-Paktika, 2023 Herat earthquake sequence, and the 2025 Kunar earthquake, did not rupture major, well-mapped faults, but instead occurred on intramountain or range-front reverse and strike-slip faults. For example, the August 31st, 2025, Mw 6.0 Kunar earthquake ruptured newly identified east–west-trending reverse fault strands at a high angle

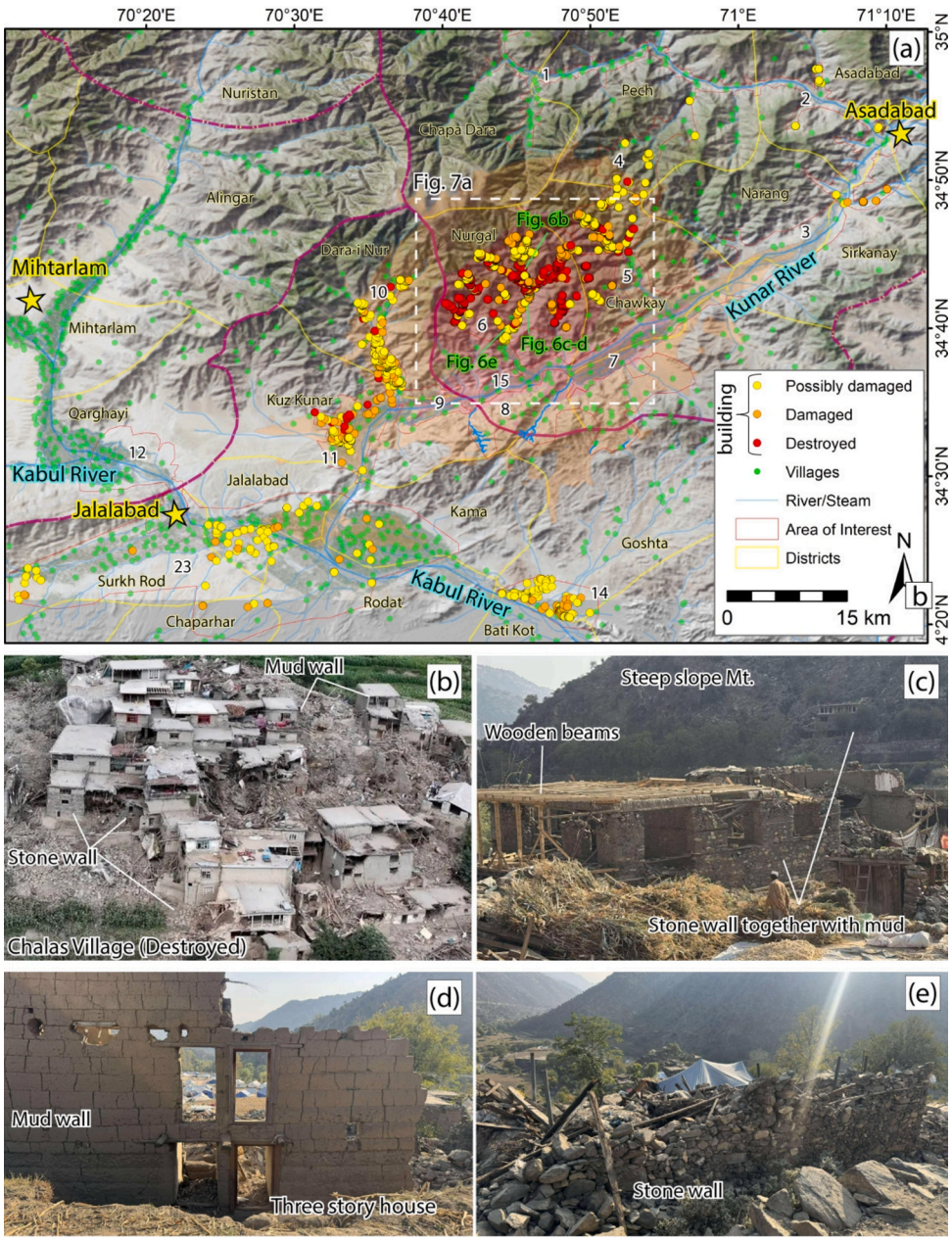


Fig. 6. (a) Distribution map of residential buildings showing destroyed, damaged, and possibly damaged structures. Most of the destroyed houses are concentrated in the epicentral area of Nurgal District, Kunar Province. The buildings data is from Copernicus Emergency Management Serivice (2025) and the background SRTM DEM from Farr et al., 2007. (b) Photograph of a severely damaged village (34°42′57.74″N, 70°45′49.66″E) called Chalas, where houses were constructed in close proximity and in stacked arrangements; the majority were destroyed during the 31 August earthquake and its aftershocks. (c) Stone masonry houses with minimal mud mortar, located on steep slopes at high elevations in the Mazar Dara Valley, Nurgal District, which collapsed during the earthquake. (d) Mud wall exhibiting multiple construction layers (paskhah technique) from a three-story building that failed during the earthquake. (e) Collapsed dry-stone wall constructed without cement or mud mortar.

within the steep terrain of the southern Hindu Kush Mountains, which had not been previously mapped and were identified here using 1-arc-second SRTM anaglyphs and satellite imagery. Similar behaviour has been documented elsewhere in the region, including the 2012 Ahar earthquakes, the 2005 Dahuiyeh (Zarand) earthquake, the 2013 Mw 6.1 Minab earthquake in Iran, all of which ruptured intramountain or subsidiary fault splays with limited geomorphic expression (Copley et al., 2013; Penney et al., 2015; Talebian et al., 2006). Together, these examples demonstrate that spatially distributed deformation and strain partitioning across fault networks allow secondary faults with low slip rates and weak surface expression to accumulate sufficient strain to produce damaging earthquakes (e.g., Copley et al., 2013; Talebian et al., 2006). Our observations of the 2025 Kunar earthquake indicate that the resulting deformation was not confined to a single mapped strand of the Kunar Fault system, but instead it was distributed over a wider structural zone, showing significant deformation gradients should be linked to subsidiary fault splays in Nuristan block. In eastern Afghanistan, close to the India-Eurasia plate boundary, steep topography, complex geology, rapid erosion, landsliding, and long recurrence intervals further obscure faults activity, causing such faults to be underrepresented in geomorphic mapping and geodetic models despite their significant seismic hazard.

The Kunar fault system plays a significant role in shaping the regional tectonics, influencing seismic activity and contributing to the rugged topography of the area. Additionally, the interaction between

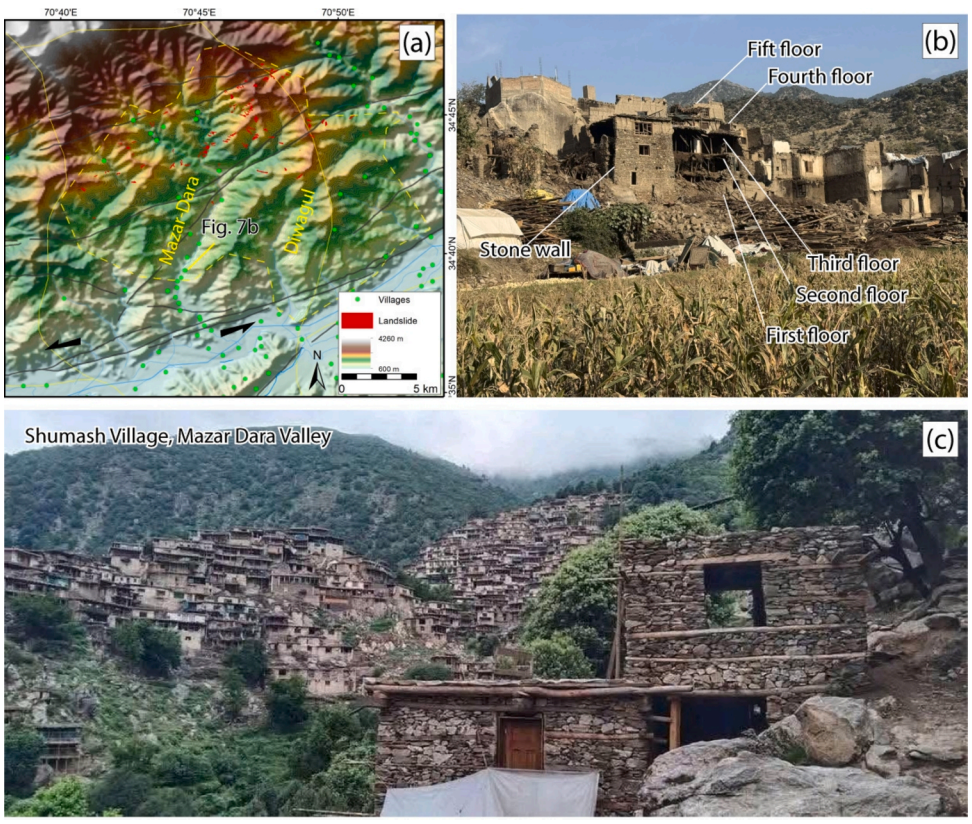


Fig. 7. **(a)** Landslide distribution map showing that most landslides occurred in Nurgal District. The landslide inventory was produced by the Copernicus Emergency Management Service using high-resolution Pleiades and WorldView satellite imagery with a spatial resolution of approximately 0.5 m. In the Nurgul District more than 100 landslides occurred during the earthquake and subsequent aftershocks. **(b)** This image shows a destroyed village in Nurgal District, with multi-story adobe buildings designed in a tradition style. **(c)** Photo of a village in eastern Afghanistan, where most houses are constructed on steep terrain, often as multi-story buildings stacked closely on top of one another.

these faults and the surrounding geological structures has led to localized zones of intense deformation. Close to the epicentral area, the Indian Plate moves at a rate of ~ 4 cm/yr beneath Eurasia (DeMets et al., 2010; Wheeler et al., 2005), which results in ongoing crustal deformation and frequent destructive earthquakes, making the region particularly susceptible to earthquake hazards (Dewey, 2006; Shnizai, 2020; Shnizai and Walker, 2024). Crustal earthquakes are concentrated around the Spin Ghar, Kunar, and Nuristan faults blocks near plate-boundary structures (Fig. 8a), in contrast to deeper seismic activity beneath the Pamir and Hindu Kush regions, which reflects ongoing mantle-scale deformation within the collision zone (e.g., Hopper et al., 2006; Prevot et al., 1980; Wheeler et al., 2005).

5.3. *Regional crustal deformation and seismotectonic implications*

Near the epicentral region localized pre-seismic uplift (~2 mm/yr) was identified, suggesting ongoing shallow deformation and highlighting the area's tectonic activity (He et al., 2026). According to the He et al. (2026), widespread subsidence occurs along the Kunar fault, in the region, including the Asadabad capital of the Kunar Province and ~ 40 km away from epicentral area. This contrast with the localized uplift at the epicentre, which remains distinct from surrounding deformation patterns. Broadly, the contemporary vertical deformation field across Afghanistan and the broader Central Asian region reflects an interplay between tectonic uplift and hydrologically driven subsidence, with the latter progressively amplified by sustained groundwater withdrawal and prolonged drought conditions in recent years (e.g., He et al., 2025; Kakar et al., 2025; Payne et al., 2025).

Deformation in eastern Afghanistan is governed by a complex tectonic framework in which oblique convergence between the two plates is accommodated through strain partitioning (Fig. 8a). Regional shortening is expressed by thrusting and folding, contributing to the uplift of major ranges such as the Spin Ghar Mountains and the Sulaiman Fold-Thrust Belt (Shnizai and Walker, 2024) (Fig. 8a-8b). At the same time, lateral shear is localized along major strike-slip fault systems, reflecting the mechanical rigidity of the crustal blocks trapped between the converging plates (e.g., Fig. 8b). This configuration promotes eastward lateral extrusion of the Jalalabad Basin between the right-lateral Spin Ghar Fault and the left-lateral Kunar Fault (Fig. 8a). The presence of the Hindu Kush and Spin Ghar ranges inhibits northward displacement, resulting instead in compression, block rotation, and lateral translation of the Kunar Block, consistent with observed geomorphic lineaments and fault-controlled basin development. The Kunar Fault initiated as a conjugate fault alongside the Spin Ghar Fault, influenced by the clockwise rotation of the block adjacent to the Peshawar Plateau (Fig. 8a-8b). The Jalalabad Basin demonstrates that the Kunar Fault shifts left, creating a pull-apart basin.

Shallow seismicity is strongly associated with major active fault systems, including the Chaman, Kunar, Gardez, Herat, and Darvaz faults, with the Chaman and Kunar faults displaying the highest levels of activity (Shareq, 1993, 1981) (Fig. 1a). Active faulting has driven uplift of the Hindu Kush and Spin Ghar ranges and controlled the formation of fault-bounded basins such as the Jalalabad Basin (e.g., Shnizai 2020; Shnizai and Walker 2024). The Kunar and Spin Ghar fault systems comprise strike-slip to oblique-slip strands with clear evidence of Quaternary activity preserved in basin sediments (e.g., Shnizai & Walker 2024). Seismological observations document teleseismic and microseismic activity aligned along the Kunar Fault and adjacent structures, with focal-mechanism solutions indicating nodal planes parallel to fault strike, confirming ongoing fault motion (Prevot et al., 1980; Quittmeyer

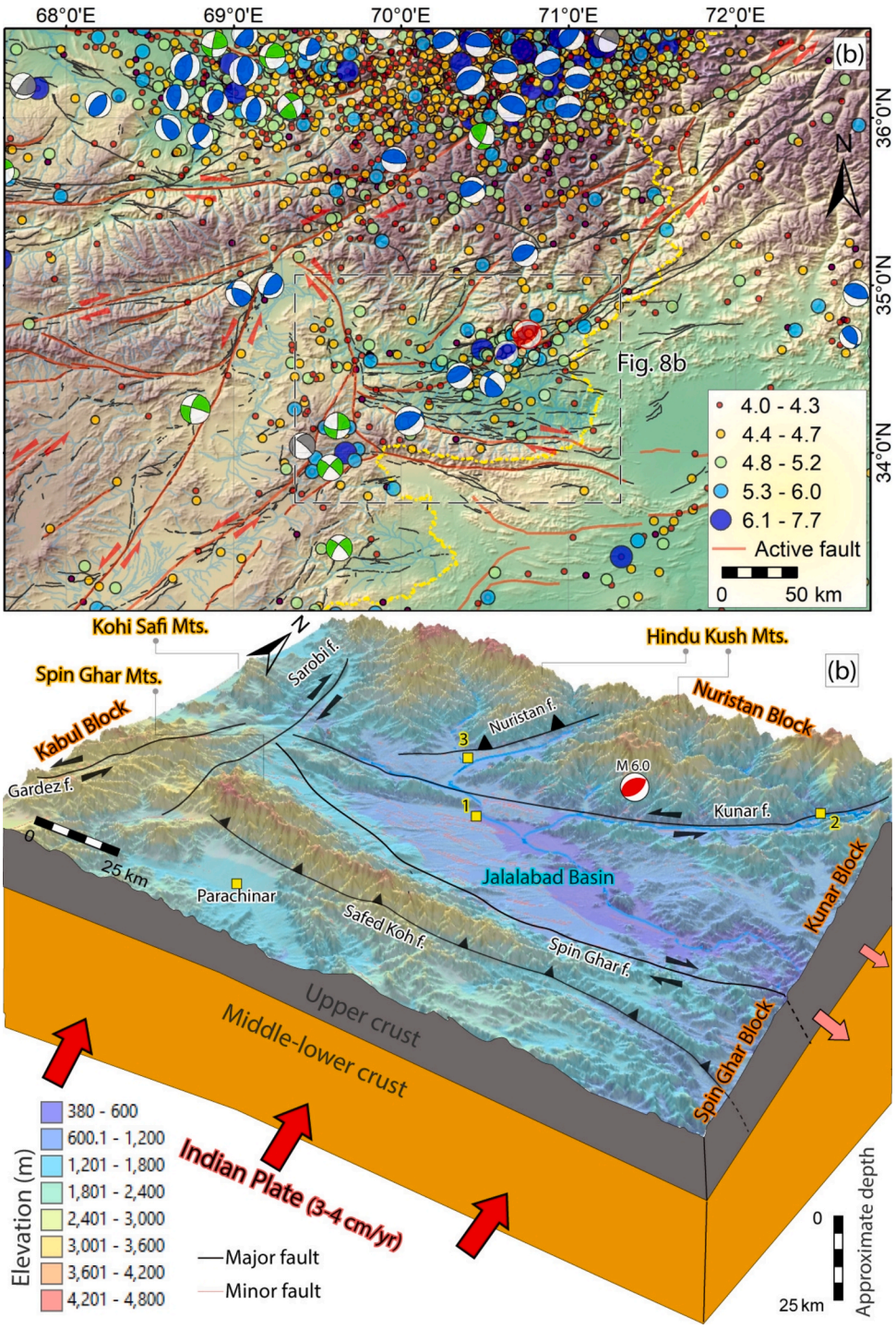


Fig. 8. (a) Seismicity map of eastern and northeastern Afghanistan based on the USGS earthquake catalogue, (Ekström et al. 2012; https://www.globalcmt.org/CMTsearch.html; USGS 2025b) including crustal seismicity at depths < 40 km with magnitudes M ≥ 4 from 1964 to the present. Focal mechanisms from the Global CMT catalogue (https://www.globalcmt.org/CMTsearch.html; Ekström et al., 2012) indicate predominantly east–west–oriented thrust faulting in the Jalalabad Basin and Spin Ghar Mountains, extending north-northeastward into the Nuristan Block. This pattern reflects ongoing convergence between the Indian and Eurasian plates, accommodated by active deformation in eastern Afghanistan. The focal mechanisms also show strike-slip faulting with both right- and left-lateral components, and shallow seismicity is spatially associated with the major mapped faults. (b) Three-dimensional perspective view based on the SRTM 1-arcsecond digital elevation model illustrating active faults, including the V-shaped conjugate Spin Ghar and Kunar strike-slip fault systems in eastern Afghanistan; the location of the 3D view is indicated in Fig. 8a. Background SRTM DEMs from Farr et al., 2007. Yell squares with black borders (1–3), indicates the provincial capitals Jalalabad, Asadabad and Mihtarlam, respectively.

and Jacob, 1979). Although west-trending thrust systems such as the Main Boundary and Safed Koh faults operate as active south-verging duplex structures (Ruleman et al., 2007), geomorphic expressions of fault activity are locally subtle and slip rates remain poorly constrained. Therefore, the seismic hazard in eastern Afghanistan may not be accurately represented by individual mapped fault traces, as coseismic strain seems to be distributed across a broader area along the Kunar-Spin Ghar structural corridor (e.g., Torabi et al., 2026). This uncertainty highlights

the need for quantitative dating of displaced Quaternary landforms to better assess seismic hazard in the Jalalabad Basin and surrounding regions.

6. Conclusion

A shallow earthquake (Mw 6.0) struck Kunar Province, Afghanistan, on 31 August at 23:47 local time, with a focal depth of 8 km. The earthquake and its aftershocks caused widespread damage across eastern Afghanistan, particularly in the provinces of Kunar, Nangarhar, and parts of Laghman. One of the largest aftershocks with a Mw 5.6 on 4 September, further intensified the impacts. The disaster resulted in over 2,200 fatalities, extensive damage to infrastructure, and the destruction of approximately 7,000 homes, either partially or completely. Ascending and descending InSAR interferograms show distinct coseismic deformation patterns associated the Mw 6.0 mainshock on 31 August and the Mw 5.6 aftershock of 4 September. The mainshock produced a broad (~12 km × 9 km), heterogeneous uplift-dominated deformation field with a maximum LOS displacement of ~ 22 cm east of Ghaziabad, whereas the aftershock generated a compact, westward-shifted, elliptical deformation pattern (~9 km × 5 km) with a NEE-trending long axis and peak displacement of ~ 15 cm, consistent with reverse faulting on a moderate-sized structure. The complexity of the mainshock deformation may reflect rupture involving structurally segmented or multiple fault strands. However, the detailed geometry of the seismogenic fault and the associated slip distribution remain to be further constrained by future quantitative geodetic fault modelling and slip inversion. Additionally, more than 104 landslides were triggered in Mazar Dara valley of the Nurgal District, Kunar Province. Generally, Eastern Afghanistan is highly prone to seismic activity due to its proximity to major fault lines, including those running through the Hindu Kush ranges, such as the Spin Ghar and Kunar fault systems. The region's complex tectonics are shaped by oblique subduction between tectonic plates, which has formed the mountains bounded by east–west and northeast-striking faults.

CRediT authorship contribution statement

Zakeria Shnizai: Writing – review & editing, Visualization, Validation, Resources, Investigation, Formal analysis, Conceptualization. **Zhenjiang Liu:** Writing – review & editing, Software, Formal analysis, Data curation. **Richard T Walker:** Writing – review & editing, Supervision, Methodology, Formal analysis, Conceptualization. **Hamidullah Waizy:** Writing – review & editing, Visualization, Investigation, Conceptualization. **Ekbal Hussain:** Writing – review & editing, Validation, Conceptualization.

Funding

The authors declare that no specific funds were received during the preparation of this manuscript.

Declaration of competing interest

The authors declare that they have no known competing financial interests or personal relationships that could have appeared to influence the work reported in this paper.

Acknowledgement

We would like to express our profound gratitude to St. Johns College Oxford for supporting Z. Shnizai through a post-doctoral fellowship. We extend our heartfelt gratitude to Sanaullah Majidi, Mohammad Omar Hashmi and others for their invaluable support in field data collection. We also express our appreciation to the Leverhulme Trust for funding through the EROICA program (Earthquake Ruptures of Iran and Central Asia, RPG-2018-371) and to the NERC-funded COMET initiative (GA/13/M/031) for their generous support. The author is also grateful to SRF and CARA for past support and opportunities that helped build the foundation for this research. Ekbal Hussain is supported by the British Geological Survey International NC programme "Geoscience to tackle Global Environmental Challenges", NE/X006255/1.

Data availability

Data will be made available on request.

References

Abdrakhmatov, K., Arrowsmith, R., Elliott, J., Grutzner, C., Mukambayev, A., Rizza, M., Shnizai, Z., Walker, R., Weldon, R., Wilkinson, R., 2024. Urgent need for greater earthquake resilience in continental Asia. Nat. Geosci. 17, 818–819. https://doi.org/10.1038/s41561-024-01531-0.

Abdullah, S., Chmyriov, V.M., Dronov, V.I., 2008. Geology and mineral resources of afghanistan. British Geological Survey, London.

Afghanistan Capacities Project (ACAPS), 2025. Afghnistan: Key pre-earthquake needs and implications for the earthquake response in Kunar province [WWW Document]. URL https://www.acaps.org/en/countries/archives/detail/ (accessed 1.15.26).

Akhundzadah, N.A., 2024. Earthquake Risk Increasing Severity and Urgent Need for Disaster Management in Afghanistan Earthquake Risk Increasing Severity and Urgent Need for Disaster Management in Afghanistan. https://doi.org/10.20944/preprints202409.1501.v1.

Alluqmani, A.E., Zaray, A.H., Wahidi, A.W., El-Hussain, I., Ansari, A., J.S, S., Maralapalle, V., 2026. Structural Deficiencies, Governance Challenges, and Strategies for Sustainable Seismic Resilience in Hazard-Prone Regions. Sustain. 2026, Vol. 18, Page 4565 18, 4565. https://doi.org/10.3390/SU18094565.

Ambraseys, N., Bilham, R., 2014. The tectonic setting of bamiyan and seismicity in and near afghanistan for the past twelve centuries BT - after the destruction of giant buddha statues in Bamiyan (Afghanistan). In: Margottini, C. (Ed.), In 2001: A UNESCO's Emergency Activity for the Recovering and Rehabilitation. Springer, Berlin Heidelberg, Berlin, Heidelberg, pp. 101–152. https://doi.org/10.1007/978-3-642-30051-6_6.

Ambraseys, N., Bilham, R., 2003. Earthquakes in Afghanistan. Seismol. Res. Lett. 74, 107–123. https://doi.org/10.1785/gssrl.74.2.107.

Ansari, A., Habib Zaray, A., Abdul, ·, Wahidi, W., Mamond, N., Özden, G., Pranjal Mandhaniya, ·, Ayed, ·, Alluqmani, E., 2026. Post-event investigation of multiscale failure patterns associated with the M w 6.0 2025 Nurgal-Kunar earthquake, Afghanistan 122, 27. https://doi.org/10.1007/s11069-026-07974-5.

Baird-Smith, R., 1942. Memoir on Indian earthquakes. J. Asiat. Soc. Bengal 12, 258–275.

Beun, N., Bordet, P., Carbonnel, J.P., 1979. Premières données quantitative relatives au coulissage du décrochement de Chaman (Afghanistan du sud-est). Comptes rendus l'Académie des Sci. 288, 931–934.

Chen, C.W., Zebker, H.A., 2001. Two-dimensional phase unwrapping with use of statistical models for cost functions in nonlinear optimization. J. Opt. Soc. Am. A 18. https://doi.org/10.1364/josaa.18.000338.

Copernicus, 2025. EMSR839 - Earthquake in Afghanistan [WWW Document]. URL https://mapping.emergency.copernicus.eu/activations/EMSR839/ (accessed 12.10.25).

Copley, A., Faridi, M., Ghorashi, M., Hollingsworth, J., Jackson, J., Nazari, H., Oveisi, B., Talebian, M., 2013. The 2012 august 11 ahar earthquakes: Consequences for tectonics and earthquake hazard in the turkish-iranian plateau. Geophys. J. Int. 196. https://doi.org/10.1093/gji/ggt379.

DeMets, C., Gordon, R.G., Argus, D.F., 2010. Geologically current plate motions. Geophys. J. Int. 181. https://doi.org/10.1111/j.1365-246X.2009.04491.x.

Denikaev, S.S., Feoktistov, V.P., Rossovsky, L.N., Adjuruddin., A., 1972. Geology and minerals in the northern part of Eastern Afghanistan. Kabul.

Dewey, J.W., 2006. Seismicity of Afghanistan and vicinity. Geol Surv Open-File Rep 2006–1185 (28), 1–55. https://doi.org/10.3133/ofr20061185.

Ekström, G., Nettles, M., Dziewoński, A.M., 2012. The global CMT project 2004-2010: Centroid-moment tensors for 13,017 earthquakes. Phys. Earth Planet. In. 200–201, 1–9. https://doi.org/10.1016/j.pepi.2012.04.002.

Elliott, J.R., Walters, R.J., Wright, T.J., 2016. The role of space-based observation in understanding and responding to active tectonics and earthquakes. Nat. Commun. 2016 71 7, 13844-. https://doi.org/10.1038/ncomms13844.

Farr, T.G., Rosen, P.A., Caro, E., Crippen, R., Duren, R., Hensley, S., Kobrick, M., Paller, M., Rodriguez, E., Roth, L., Seal, D., Shaffer, S., Shimada, J., Umland, J., Werner, M., Oskin, M., Burbank, D., Alsdorf, D.E., 2007. The shuttle radar topography mission. Rev. Geophys. 45. https://doi.org/10.1029/2005RG000183.

Furuya, M., Satyabala, S.P., 2008. Slow earthquake in Afghanistan detected by InSAR. Geophys. Res. Lett. 35, 1–15. https://doi.org/10.1029/2007GL033049.

Global Disaster Awareness and Coordination System (GDACS), 2025. M 6 in Afghanistan on 31 Aug 2025 19:17 UTC [WWW Document]. URL https://www.gdacs.org/report.aspx?eventid=1498339&eventtype=EQ (accessed 1.10.26).

Goldstein, R.M., Zebker, H.A., Werner, C.L., 1988. Satellite radar interferometry: Two-dimensional phase unwrapping. Radio Sci. 23. https://doi.org/10.1029/RS023i004p00713.

He, P., Craig, T.J., Wen, Y., Weng, H., He, K., Xu, C., 2026. Multi-stage shallow rupture and pre-event shallow deformation during the 2025 Mw 5.9 Asadabad earthquake (Afghanistan). Geophys. Res. Lett. 53. https://doi.org/10.1029/2026GL121737.

He, P., Wen, Y., Zhong, Y., Cai, J., 2025. Nonoverlapped sources of the Devastating 2023 Mw >6 Herat, Afghanistan, Earthquake Swarm estimated by InSAR. Seismol. Res. Lett. 96, 838–847. https://doi.org/10.1785/0220240239.

Heuckroth, L.E., Karim, R.A., 1970. Earthquake history, seismicity, and tectonics of the regions of Afghanistan. Kabul Univ. 202.

Hopper, M.G., Rukstales, K.S., Johnson, M.L., Dewey, J.W., Bergman, E.A., Sipkin, S.A., 2006. Damaging Historical Earthquakes in the Afghanistan Region. U.S. Geol. Surv. Open-File Rep. 2006–1185 Plate 2 2.

Kakar, N., Metzger, S., Schöne, T., Motagh, M., Waizy, H., Nasrat, N.A., Lazecký, M., Amelung, F., Bookhagen, B., 2025. Interferometric radar satellite and in-situ well time-series reveal groundwater extraction rate changes in urban and rural Afghanistan. Water Resour. Res. 61. https://doi.org/10.1029/2023WR036626.

Li, Z., Wright, T., Hooper, A., Crippa, P., Gonzalez, P., Walters, R., Elliott, J., Ebmeier, S., Hatton, E., Parsons, B., 2016. TOWARDS INSAR EVERYWHERE, ALL THE TIME, WITH SENTINEL-1. Int. Arch. Photogramm. Remote Sens. Spat. Inf. Sci. XLI-B4. https://doi.org/10.5194/isprs-archives-xli-b4-763-2016.

Liu, Z., Li, Z., Yu, C., Song, C., Wang, J., Zhang, X., Hu, X., Peng, J., 2025. Coseismic rupture and early afterslip of the 2023 herat (Afghanistan) earthquake sequence: Insights from sentinel-1 radar observations. J. Geophys. Res. Solid Earth 130. https://doi.org/10.1029/2024JB029495.

Mohadjer, S., Bendick, R., Ischuk, A., Kuzikov, S., Kostuk, A., Saydullaev, U., Lodi, S., Kakar, D.M., Wasy, A., Khan, M.A., Molnar, P., Bilham, R., Zubovich, A.V., 2010. Partitioning of India-Eurasia convergence in the Pamir-Hindu Kush from GPS measurements. Geophys. Res. Lett. 37, 1–6. https://doi.org/10.1029/2009GL041737.

Mohammadi, A., Mansouri, R., Shokri-Kaveh, M., Shnizai, Z., 2026. Seismotectonic framework of Afghanistan: An Integrated review of geology, active tectonics, and crustal structure using gravity data. Pure Appl. Geophys. 2026, 1–32. https://doi.org/10.1007/s00024-025-03904-x.

Nakata, T., Tsutsumi, H., Khan, S.H., Lawrence, R.D., 1991. Active faults of Pakistan: map sheets and inventories (special Publication). Res. Cent. Reg. Geogr. Hiroshima Univ. 21, 141.

OCHA (United Nations for the Coordination of Humanitarian Affairs), 2025. Afghanistan: Flash Update #6 Earthquake in Nangarhar Province.

Payne, J.A., Watson, A.R., Maghsoudi, Y., Ebmeier, S.K., Rigby, R., Lazecký, M., Thomas, M., Elliott, J.R., 2025. Widespread Extent of irrecoverable aquifer depletion revealed by country-wide analysis of land surface subsidence hazard in Iran. J. Geophys. Res. Solid Earth 130. https://doi.org/10.1029/2024JB030367.

Penney, C., Copley, A., Oveisi, B., 2015. Subduction tractions and vertical axis rotations in the Zagros-Makran transition zone, SE Iran: The 2013 May 11 Mw 6.1 Minab earthquake. Geophys. J. Int. 202. https://doi.org/10.1093/gji/ggv202.

Prevot, R., Hatzfeld, D., Roecker, S.W., Molnar, P., 1980. Shallow earthquakes and active tectonics in eastern Afghanistan. J. Geophys. Res. 85, 1347–1357. https://doi.org/10.1029/JB085iB03p01347.

Quittmeyer, R.C., Jacob, K.H., 1979. Historical and modern seismicity of Pakistan, Afghanistan, northwestern India, and southeastern Iran. Bull. Seismol. Soc. Am. 69, 773–823.

Reliefweb, 2025. Afghanistan: Eastern Region Earthquake Situation Report #3, September 10, 2025.

Ruleman, C.A., Crone, A.J., Machette, M.N., Haller, K.M., Rukstales, K.S., 2007. Map and Database of Probable and Possible Quaternary Faults in Afghanistan, 1:. Open-File Report.

Scheiber, R., Moreira, A., 2000. Coregistration of interferometric SAR images using spectral diversity. IEEE Trans. Geosci. Remote Sens. 38. https://doi.org/10.1109/36.868876.

Shareq, A., 1993. Seismic hazard assessment in the Islamic state of Afghanistan, in: McGuire, R.K. (Ed.), The Practice of Earthquake Hazard Assessment. International Association of Seismology and Physics of the Earth's Interior, pp. 1–6.

Shareq, A., 1981. Geological Observations and Geophysical Investigations Carried out in Afghanistan over the Period of 1972–1979, in: Gupta, H.K., Delany, F.M. (Eds.), Zagros, Hindu Kush, Himalaya—Geodynamic Evolutionn. American Geophysical Union (AGU), pp. 75–86. https://doi.org/10.1029/GD003P0075.

Shirzaei, M., Mohammad Taqi Daqiq, Jonathan Lucy, Susanna Werth, Ravi Sharma, Michelle Jaramillo Velasco, Mir Matin, Kaveh Madani, 2025. Damage Assessment of Afghanistan's August 2025 Earthquake. United Nations Univ. Water, Environ. Heal. 1–6. https://doi.org/10.53328/INR25MSIR002.

Shnizai, Z., 2020. Mapping of active and presumed active faults in Afghanistan by interpretation of 1-arcsecond SRTM anaglyph images. J. Seismol. https://doi.org/10.1007/s10950-020-09933-4.

Shnizai, Z., Matsushi, Y., Tsutsumi, H., 2020. Late Pleistocene slip rate of the Chaman fault based on 10Be exposure dating of offset geomorphic surfaces near Kabul, Afghanistan. Tectonophysics 795, 1–14. https://doi.org/10.1016/j.tecto.2020.228593.

Shnizai, Z., Talebian, M., Valkanotis, S., Walker, R., 2022. Multiple factors make Afghan communities vulnerable to earthquakes. Temblor. https://doi.org/10.32858/temblor.266.

Shnizai, Z., Walker, R., 2024. Detailed mapping of the spin Ghar active fault system in eastern Afghanistan based on satellite image interpretation. Tektonika 2, 132–156. https://doi.org/10.55575/tektonika2024.2.1.49.

Shnizai, Z., Walker, R., Tsutsumi, H., 2024. The Chaman and Paghman active faults, west of Kabul, Afghanistan: Active tectonics, geomorphology, and evidence for rupture in the destructive 1505 earthquake. J. Asian Earth Sci. 259. https://doi.org/10.1016/j.jseaes.2023.105925.

Talebian, M., Biggs, J., Bolourchi, M., Copley, A., Ghassemi, A., Ghorashi, M., Hollingsworth, J., Jackson, J., Nissen, E., Oveisi, B., Parsons, B., Priestley, K., Saiidi, A., 2006. The Dahuiyeh (Zarand) earthquake of 2005 February 22 in central Iran: Reactivation of an intramountain reverse fault. Geophys. J. Int. 164. https://doi.org/10.1111/j.1365-246X.2005.02839.x.

Tapponnier, P., Mattauer, M., Proust, F., Cassaigneau, C., 1981. Mesozoic ophiolites, sutures, and arge-scale tectonic movements in Afghanistan. Earth Planet. Sci. Lett. 52, 355–371. https://doi.org/10.1016/0012-821X(81)90189-8.

Torabi, H., Kandregula, R.S., Naik, S.P., Shnizai, Z., Ghildiyal, D., Chufal, V.S., Kim, Y.-S., 2026. Evidence for Distributed Transpressional Deformation and Seismic Hazard Implications from the 2025 Mw 6.0 Asadabad- Kunar Earthquake, Eastern Afghanistan. Nat. Hazar. https://doi.org/10.21203/rs.3.rs-9452025/v1.

Treloar, P.J., Izatt, C.N., 1993. Tectonics of the Himalayan collision between the Indian plate and the afghan block: A synthesis. Geol. Soc. Spec. Publ. 74, 69–87. https://doi.org/10.1144/GSL.SP.1993.074.01.06.

United Nations Satellite Centre (UNOSAT), 2025. Damage Assessment in Jalalabad City, Nangarhar Province as of 2 September 2025 [WWW Document]. accessed 1.10.26. https://unosat.org/products/4196.

U.S. Geological Survey (USGS), 2025a. M 6.0 - 35 km WSW of Asadābād, Afghanistan [WWW Document]. URL https://earthquake.usgs.gov/earthquakes/eventpage/us7000qsvj/executive (accessed 11.1.25).

U.S. Geological Survey (USGS), 2025b. Earthquake Catalog [WWW Document]. URL https://earthquake.usgs.gov/earthquakes/search/ (accessed 11.20.25).

Verma, R.K., Mukhopadhyay, M., Bhanja, A.K., 1980. Seismotectonics of the Hindukush and Baluchistan arc. Test Tectonophys. 66. https://doi.org/10.1016/0040-1951(80)90247-4.

Waizy, H., Shnizai, Z., Omid, M.W., Ahmadi, R.G., Naing, T.T., 2025. A multi-method approach to the investigation of Kunar marble deposits. Eastern Afghanistan. Moscow Univ. Geol. Bull. 80, 456–475. https://doi.org/10.3103/S0145875225700607.

Wegnüller, U., Werner, C., Strozzi, T., Wiesmann, A., Frey, O., Santoro, M., 2016. Sentinel-1 Support in the GAMMA Software, in: Procedia Computer Science. https://doi.org/10.1016/j.procs.2016.09.246.

Wheeler, R.L., Bufe, C.G., Johnson, M.L., Dart, R.L., 2005. Seismotectonic Map of Afghanistan, with annotated bibliography. US Geol Surv Open-File Rep 2007–1264, 31.

Yague-Martinez, N., Prats-Iraola, P., Gonzalez, F.R., Brcic, R., Shau, R., Geudtner, D., Eineder, M., Bamler, R., 2016. Interferometric processing of sentinel-1 TOPS data. IEEE Trans. Geosci. Remote Sens. 54. https://doi.org/10.1109/TGRS.2015.2497902.

Yu, C., Li, Z., Penna, N.T., 2018a. Interferometric synthetic aperture radar atmospheric correction using a GPS-based iterative tropospheric decomposition model. Remote Sens. Environ. 204. https://doi.org/10.1016/j.rse.2017.10.038.

Yu, C., Li, Z., Penna, N.T., Crippa, P., 2018b. Generic Atmospheric Correction Model for Interferometric Synthetic Aperture Radar Observations. J. Geophys. Res. Solid Earth 123. https://doi.org/10.1029/2017JB015305.

Yu, C., Penna, N.T., Li, Z., 2017. Generation of real-time mode high-resolution water vapor fields from GPS observations. J. Geophys. Res. 122. https://doi.org/10.1002/2016JD025753.